Antenna Position Estimation Through Subsampled Exponential Analysis of Signals in the Near Field

Ridalise Louw, Ferre Knaepkens, Annie Cuyt, Wen-shin Lee, Stefan J. Wijnholds, Dirk I. L. de Villiers, and Rina-Mari Weideman

Abstract – In a previous article we explored the use of a subsampled exponential analysis algorithm to find the antenna-element positions in a large irregular planar array after the installation phase. The application requires an unmanned aerial vehicle to be flown over the antenna array while transmitting several odd harmonic signals. The received signal samples at a chosen reference antenna element are then compared to those at every other element in the array in order to find its position. Previously, the far-field approximation was used to calculate the time delay between received signals. In this article the method is reconsidered for the more realistic case of when the source is in the near field of the array. A number of problems that arise are addressed, and results from a controlled simulation are presented to illustrate that the computational method works.

1. Introduction

Ensuring accurate placement of the antenna elements in large-*N* radio interferometers like the Low Frequency Array (LOFAR) [1] and the Square Kilometre Array [2] is a costly and time-consuming process. Methods for finding the positions of individual antenna elements within an irregular array after the installation phase have been proposed [3, 4] in which signals are transmitted from an unmanned aerial vehicle (UAV) toward the array. This saves time and money by allowing for errors from the designed positions during placement of the elements, as well as indicating which elements are connected incorrectly to the back end. The application of a subsampled exponential analysis algorithm using the far-field approximation was presented in [4]. Here the method is extended for when the UAV is in the near field of the array.

Manuscript received 28 December 2021.

Ridalise Louw, Dirk de Villiers, and Rina-Mari Weideman are with the Department of Electrical and Electronic Engineering, Stellenbosch University, Cnr Banghoek Road & Joubert Street, Stellenbosch, 7600, South Africa; e-mail: 17002567@sun.ac.za, ddv@sun.ac.za, 18954626@sun.ac.za.

Ferre Knaepkens is with the Department of Computer Science, University of Antwerp, Middelheimlaan 1, 2020 Antwerpen, Belgium; e-mail: ferre.knaepkens@uantwerpen.be.

Annie Cuyt is with the Department of Computer Science, University of Antwerp, Middelheimlaan 1, 2020 Antwerpen, Belgium, and the College of Mathematics and Statistics, Shenzhen University, Shenzhen, Guangdong 518060, China; e-mail: annie.cuyt@uantwerpen.be.

Wen-shin Lee is with the Division of Computing Science and Mathematics, University of Stirling, Stirling FK9 4LA, Scotland (UK), and the Department of Computer Science, University of Antwerp, Middelheimlaan 1, 2020 Antwerpen, Belgium; e-mail: wen-shin.lee@stir.ac.uk.

Stefan Wijnholds is with the Netherlands Institute for Radio Astronomy (ASTRON), Dwingeloo, The Netherlands, and the Department of Electrical and Electronic Engineering, Stellenbosch University, Stellenbosch 7600, South Africa; e-mail: wijnholds@astron.nl.

2. Problem Formulation

Figure 1 illustrates narrowband odd harmonic signals $S_i(t_p)$ transmitted from the UAV when it is located at position $\mathbf{r}_p$ at time t_p. The index $i \in \mathbb{N}$ distinguishes between frequencies $\omega_i = (2i + 1)\omega_0$, where ω_0 is the baseband frequency. At time t_p, the signals are expressed as

$$S_i(t_p) = s_i(t_p) \exp(j\omega_i t_p) \tag{1}$$

where $s_i(t_p)$ is assumed to remain constant during the measurement of $S_i(t_p)$. As in [3, 4], we assume the signals are strong enough that astronomical sources in the field of view of the array can be ignored. With the UAV in the radiating near field of the antenna, a curved phase front is incident on the array.

A reference antenna element $\mathbf{a}_1 = (0, 0, 0)$ is chosen to coincide with the origin. All elements are assumed to be located in the (x, y)-plane, so their z-coordinates are zero. In the near field, the time delay of incidence on the mth antenna element at position $\mathbf{a}_m = u_m\mathbf{x} + v_m\mathbf{y} + (0)\mathbf{z}$ relative to $\mathbf{a}_1$ at time t_p is

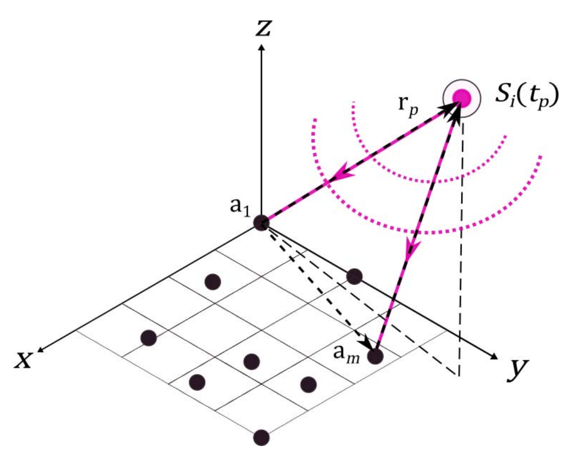

Figure 1. The UAV transmits signals $S_i(t_p)$ at time t_p while in the near field of the planar array.

$$\tau_m(x_p, y_p, z_p) = \frac{\|\mathbf{r}_p\| - \|\mathbf{r}_p - \mathbf{a}_m\|}{c} = \frac{r_p - \sqrt{r_p^2 + u_m^2 + v_m^2 - 2(u_m x_p + v_m y_p)}}{c} \tag{2}$$

where $\mathbf{r}_p = x_p\mathbf{x} + y_p\mathbf{y} + z_p\mathbf{z}$ is the vector from the origin to the UAV's position, $r_p = \|\mathbf{r}_p\|$, $\mathbf{r}_p - \mathbf{a}_m$ is the vector from the mth antenna element to the UAV, and c is the propagation velocity of the signal, or the speed of light in free space. From the narrowband assumption, the samples at the mth element at time t_p for frequency i are

$$\begin{aligned} f_{mi}(t_p) &= S_i(t_p + \tau_m(x_p, y_p, z_p)) \\ &\approx s_i(t_p)\exp(j\omega_i t_p)\exp(j\omega_i \tau_m(x_p, y_p, z_p)) \end{aligned} \tag{3}$$

To extract the positions $(u_m, v_m, 0)$, we need multiple samples at time t_p, and this from several positions $\mathbf{r}_p$, with $p = 1, \ldots, P$ [5]. We use the following shorthand notations for a fixed UAV position $\mathbf{r}_p$:

$$\begin{aligned} f_{mip} &= f_{mi}(t_p), \\ \alpha_{ip} &= s_i(t_p)\exp(j\omega_i t_p), \\ \Delta_{mp} &= u_m^2 + v_m^2 - 2(u_m x_p + v_m y_p), \\ \tau_{mp} &= \tau_m(x_p, y_p, z_p) = \frac{1}{c}\left(r_p - \sqrt{r_p^2 + \Delta_{mp}}\right), \\ \Psi_{mp} &= j\omega_0 \tau_{mp} \text{ so that } (2i+1)\Psi_{mp} = j\omega_i \tau_{mp} \end{aligned} \tag{4}$$

The samples at each element m are filtered into subbands, so for position p,

$$f_{mip} = \alpha_{ip}\exp((2i+1)\Psi_{mp}) \tag{5}$$

The frequency and positional dependence of the coefficients α_{ip} are undesirable. Therefore, we first divide the sample sets f_{mip} by the reference antenna element's samples $f_{1ip} = s_i(t_p)\exp(j\omega_i t_p)\exp(0) = \alpha_{ip}$, which gives

$$f'_{mip} = \frac{f_{mip}}{f_{1ip}} = \exp((2i+1)\Psi_{mp}) \tag{6}$$

3. Subsampled Exponential Analysis

To ensure that no aliasing occurs, we need $|2\Psi_{mp}| < \pi$, which leads to the spatial Nyquist criterion

$$\left|2\left(r_p - \sqrt{r_p^2 + \Delta_{mp}}\right)\right| < \frac{\lambda_0}{2} \tag{7}$$

where λ_0 is the wavelength of ω_0. In the dense case where (7) holds, the base terms Ψ_{mp} can be recovered from the signal samples by using any Prony-like method. If (7) is not satisfied, we have a subsampled exponential analysis problem that we can solve with a technique similar to [6, 7]. This dealiasing method works with coprime scale parameters σ_1 and σ_2 and can also be used in the multivariate case [5]. The equations for the near-field base terms Ψ_{mp} in (4) are nonlinear, so in order to recover from aliasing using this approach, we first linearize our model with a first-order Taylor-series partial sum.

4. Linearization of the Near-Field Model

While u_m and v_m denote the coordinates of antenna element $\mathbf{a}_m$ in the (x,y)-plane and (x_p, y_p, z_p) denotes the location of the UAV in space at time t_p, we introduce the general coordinates u and v in the plane. During the linearization, we keep $\mathbf{r}_p = x_p\mathbf{x} + y_p\mathbf{y} + z_p\mathbf{z}$ at time t_p fixed, so that the expression

$$\begin{aligned} g_p(u, v) &= \|\mathbf{r}_p\| - \sqrt{\|\mathbf{r}_p\|^2 + \Delta_p(u, v)}, \\ \Delta_p(u, v) &= u^2 + v^2 - 2(u x_p + v y_p) \end{aligned}$$

varies only with the planar position (u, v). We approximate $g_p(u, v)$ by

$$\begin{aligned} L_p(u, v) = g_p(\tilde{u}, \tilde{v}) &+ (u - \tilde{u}) g_p^{(u)}(\tilde{u}, \tilde{v}) \\ &+ (v - \tilde{v}) g_p^{(v)}(\tilde{u}, \tilde{v}) \end{aligned} \tag{8}$$

where $g_p^{(u)}$ and $g_p^{(v)}$ are the partial derivatives with respect to u and v,

$$\begin{aligned} g_p^{(u)}(u, v) &= \frac{x_p - u}{\sqrt{\|\mathbf{r}_p\|^2 + \Delta_p(u, v)}}, \\ g_p^{(v)}(u, v) &= \frac{y_p - v}{\sqrt{\|\mathbf{r}_p\|^2 + \Delta_p(u, v)}} \end{aligned} \tag{9}$$

Substituting these equations into (8), the linearized approximation $L_p(u, v)$ becomes

$$\begin{aligned} L_p(u, v) = r_p - \sqrt{r_p^2 + \Delta_p(\tilde{u}, \tilde{v})} &+ \frac{(u - \tilde{u})(x_p - \tilde{u})}{\sqrt{r_p^2 + \Delta_p(\tilde{u}, \tilde{v})}} \\ &+ \frac{(v - \tilde{v})(y_p - \tilde{v})}{\sqrt{r_p^2 + \Delta_p(\tilde{u}, \tilde{v})}} \end{aligned} \tag{10}$$

Let the constant terms in (10), for a certain estimation $(\tilde{u}, \tilde{v})$, be denoted by

$$\begin{aligned} \kappa_p(\tilde{u}, \tilde{v}) = r_p &- \sqrt{r_p^2 + \Delta_p(\tilde{u}, \tilde{v})} \\ &- \frac{\tilde{u}(x_p - \tilde{u}) + \tilde{v}(y_p - \tilde{v})}{\sqrt{r_p^2 + \Delta_p(\tilde{u}, \tilde{v})}} \end{aligned} \tag{11}$$

Then we can use the remaining function

$$L_p(u, v) - \kappa_p(\tilde{u}, \tilde{v}) = \frac{u(x_p - \tilde{u}) + v(y_p - \tilde{v})}{\sqrt{r_p^2 + \Delta_p(\tilde{u}, \tilde{v})}} \tag{12}$$

to solve the positions of the elements in the antenna array in the near-field sub-Nyquist case, where the common factor $1\big/\sqrt{r_p^2 + \Delta_p(\tilde{u}, \tilde{v})}$ can be used to model σ_j, $j = 1, 2$, as explained in the next section.

5. Exponential Analysis of the Linearized Near-Field Problem

Choose $2P$ radial positions $\mathbf{r}_{p_j} = x_p\mathbf{x} + y_p\mathbf{y} + z_{p_j}\mathbf{z}$ with radial distance $r_{p_j} = \|\mathbf{r}_{p_j}\|$, for $j = 1$, 2 and $p = 1, \ldots, P$. Let $\tilde{u}_m$ and $\tilde{v}_m$ be estimates of the coordinates u_m and v_m in the (x, y)-plane of antenna $\mathbf{a}_m$, and let us denote $\tilde{\Delta}_{mp} = \Delta_p(\tilde{u}_m, \tilde{v}_m)$ and $\kappa_{mp_j} = \kappa_{p_j}(\tilde{u}_m, \tilde{v}_m)$. Note that $\tilde{\Delta}_{mp}$ is independent of the z-coordinate and therefore simply indexed by p, not p_j. With p and m fixed, the linearization

$$L_{p_j}(u_m, v_m) - \kappa_{mp_j} = \frac{u_m(x_p - \tilde{u}_m) + v_m(y_p - \tilde{v}_m)}{\sqrt{r_{p_j}^2 + \tilde{\Delta}_{mp}}} \tag{13}$$

is used to model the near-field nonlinear

$$g_{p_j}(u_m, v_m) = r_{p_j} - \sqrt{r_{p_j}^2 + \Delta_{mp}} \approx L_{p_j}(u_m, v_m) \tag{14}$$

The approximation in the right-hand side of (14) becomes more accurate as the value of $(\tilde{u}_m, \tilde{v}_m)$ gets closer to the true antenna element position (u_m, v_m). We additionally introduce the virtual UAV position $\mathbf{R}_p = x_p\mathbf{x} + y_p\mathbf{y} + Z_p\mathbf{z}$ with virtual height Z_p and $R_p = \|\mathbf{R}_p\|$, such that the spatial Nyquist criterion

$$\left|2\left(R_p - \sqrt{R_p^2 + \Delta_{mp}}\right)\right| < \frac{\lambda_0}{2} \tag{15}$$

is met for all m. With R_p, we rewrite the value C_{mp_j} as a scaled C_{mp},

$$\begin{aligned} C_{mp_j} &= \frac{1}{\sqrt{r_{p_j}^2 + \tilde{\Delta}_{mp}}} = \sigma_{jmp} C_{mp}, \\ C_{mp} &= \frac{1}{\sqrt{R_p^2 + \tilde{\Delta}_{mp}}} \end{aligned} \tag{16}$$

and we start the iterative improvement of the estimation $(\tilde{u}_m, \tilde{v}_m)$. During the iteration, the values of r_{p_j} remain constant while $\tilde{\Delta}_{mp}$ is updated at every iteration step. The values of σ_{jmp} and R_p are manipulated in every iteration step to give (16), with the only restrictions being that the spatial Nyquist criterion in (15) must be met and σ_{jmp}, $j = 1$, 2 must be coprime in order to recover from aliasing. If we set $r_{p_1} > r_{p_2}$, then $C_{mp_2} > C_{mp_1}$ for all m. The ratios

$$\frac{\sigma_{2mp}}{\sigma_{1mp}} = \frac{C_{mp_2}}{C_{mp_1}} \tag{17}$$

rounded to two significant digits provide coprime values for σ_{1mp} and σ_{2mp}. For each antenna, we start with $\tilde{u}_m = \tilde{v}_m = 0$ so that $\tilde{\Delta}_{mp} = 0$ and $\kappa_{mp} = 0$. A new value of the estimated antenna position $(\tilde{u}_m, \tilde{v}_m)$ is found as follows, using our approximated model in conjunction with the subsampled exponential algorithm.

The samples at each antenna element normalized by f_{1ip_j} according to (6) are

$$f'_{mip_j} = \exp\left((2i+1)\, j\frac{\omega_0}{c}\left(r_{p_j} - \sqrt{r_{p_j}^2 + \Delta_{mp}}\right)\right) \tag{18}$$

Thus, a priori we compute the base terms

$$\exp\left(2j\frac{\omega_0}{c}\left(r_{p_j} - \sqrt{r_{p_j}^2 + \Delta_{mp}}\right)\right) \tag{19}$$

using any Prony-like method for the samples f'_{mip_j}. Here we prefer the Root-MUSIC algorithm [8] because of its accuracy. For every antenna element $\mathbf{a}_m$, every position p, and every j we use N_t time samples of the form in (18), with added white Gaussian noise from systematic effects in the antenna array's channels. Fortunately, the noise encourages clustering in the complex plane around the true solution of the base terms in (19) [6]. We use the densest point from all evaluations as our best estimate of (19), which is defined as the point inside the smallest possible radius that contains a specified minimum number of points around it.

Subsequently, in every iteration step the estimated base terms are shifted by multiplying them with $\exp\left(-j\frac{2\omega_0}{c}\kappa_{mp_j}\right)$. Since $\Delta_{mp} \approx \tilde{\Delta}_{mp}$, we find that

$$g_{p_j}(u_m, v_m) = r_{p_j} - \sqrt{r_{p_j}^2 + \Delta_{mp}} \approx r_{p_j} - \sqrt{r_{p_j}^2 + \tilde{\Delta}_{mp}}$$

and hence that the linearization in (13) can be used. Moreover,

$$\begin{aligned} & j\frac{2\omega_0}{c}\left(r_{p_j} - \sqrt{r_{p_j}^2 + \Delta_{mp}} - \kappa_{mp_j}\right) \\ & \approx j\frac{2\omega_0}{c}\left(\frac{u_m(x_p - \tilde{u}_m) + v_m(y_p - \tilde{v}_m)}{\sqrt{r_{p_j}^2 + \tilde{\Delta}_{mp}}}\right) \\ & = j\frac{2\sigma_{jmp}\omega_0}{c}\left(\frac{u_m(x_p - \tilde{u}_m) + v_m(y_p - \tilde{v}_m)}{\sqrt{R_p^2 + \tilde{\Delta}_{mp}}}\right) \end{aligned} \tag{20}$$

We can therefore denote the left-hand side of (20) by $\sigma_{jmp}\Phi_{mp}$. The possible arguments Φ_{mp} of $\exp(\sigma_{jmp}\Phi_{mp})$ are collected in two sets ($j = 1$, 2):

$$\left\{\Phi_{mp} + \frac{j2\pi}{\sigma_{jmp}} l \;:\; l = 0, \ldots, \sigma_{jmp} - 1\right\} \tag{21}$$

Since σ_{jmp} are chosen as coprime for every m and p, the intersection of the sets (21) for $j = 1$, 2 contains the unique dealiased argument which is the valid Φ_{mp} [7].

A complication arises when trying to extract the values of (u_m, v_m) from Φ_{mp}, which is our ultimate goal. From the expression for Φ_{mp} we find

$$j\frac{c}{2\omega_0}\Phi_{mp} + \frac{r_{p_j} - \kappa_{mp_j}}{\sigma_{jmp}} = \sqrt{R_p^2 + \Delta_{mp}}$$

Inside the square root we have

$$\begin{aligned} R_p^2 + \Delta_{mp} &= x_p^2 + y_p^2 + Z_p^2 + u_m^2 + v_m^2 - 2(u_m x_p + v_m y_p) \\ &= (u_m - x_p)^2 + (v_m - y_p)^2 + Z_p^2 \end{aligned} \tag{22}$$

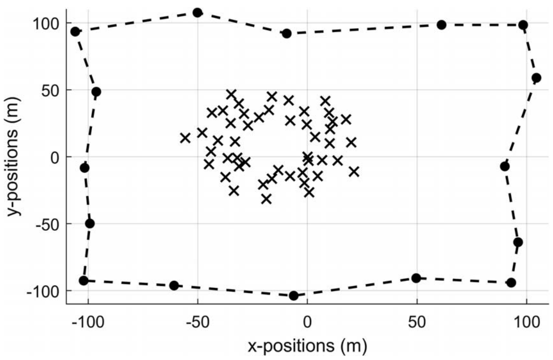

Figure 2. Antenna positions and UAV flight path.

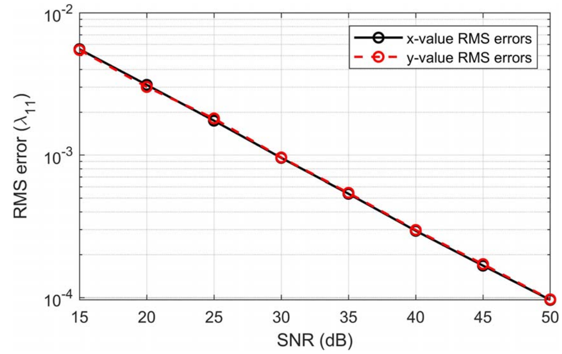

Figure 3. Root-mean-square errors of element positions in a LOFAR LBA outer substation for different noise levels using the linearized near-field model with $P = 16$ and $N_t = 80$.

Equation (22) defines a circle with center $\left(x_p, y_p\right)$ and radius $R_p^2 - Z_p^2 + \Delta_{mp}$. Thus for any two distinct positions of the UAV, the possible solutions of (u_m, v_m) occur at the intersections of two circles. To find the correct solution, we add distinct UAV positions so that $P \geq 3$ and we have $N_c = \begin{pmatrix} P \\ 2 \end{pmatrix}$ combinations of pairs of circles whose intersections are possible solutions of (u_m, v_m). We use the mean of the N_c closest intersections as the solution to (u_m, v_m), which then becomes the updated value of $(\tilde{u}_m, \tilde{v}_m)$ in the linear model in (13). The entire procedure discussed in this section is repeated until

$$\sqrt{\left(u_m - \tilde{u}_m\right)^2 + \left(v_m - \tilde{v}_m\right)^2} < 0.01 \tag{23}$$

This iterative process should converge due to the convexity of the linearized function

$$\begin{aligned} g_p(u, v) &= r_p - \sqrt{r_p^2 + u^2 + v^2 - 2\left(u x_p + v y_p\right)} \\ &= r_p - \sqrt{\left(x_p - u\right)^2 + \left(y_p - v\right)^2 + z_p^2}. \end{aligned}$$

6. Simulation Results

In practice, this method is performed off-line using the time-series signals from each antenna element in the respective frequency bins, as described in (3). To demonstrate that the algorithm works, we present results from a controlled simulation that does not include practical considerations such as mutual coupling or the precision with which the UAV's position can be determined. However, the simulation parameters are from actual in situ measurement campaigns that were performed on the LOFAR low-band antenna (LBA), such as in [9]. We use the outer LBA substation for our simulation, for which the positions of the antenna elements are indicated by the crosses in Figure 2. The flight path of the UAV is a 100 m × 100 m square, with some deviations caused by wind. The black dots indicate the $P = 16$ positions that are used.

The fifth, seventh, ninth, and 11th harmonics of the baseband frequency $f_0 = 6.3585$ MHz are transmitted from the UAV, so $i = [2,3,4,5]$. One hundred Monte Carlo runs were performed for signal-to-noise ratios (SNRs) of 15 dB to 50 dB. The number of samples at each position is $N_t = 80$. For each antenna, the median estimated position over all runs was taken and compared with the actual position. The root-mean-square (RMS) errors of the difference between the x- and y-positions for all the antenna elements were calculated at each noise level. The results are presented in Figure 3 in terms of the wavelength of the highest frequency harmonic $\lambda_{11} = 4.29$ m transmitted from the UAV. Even at an SNR of 15 dB, the RMS error is less than 1% of the smallest transmitted wavelength λ_{11}, confirming the efficacy of the computational method.

7. Conclusion

This article expands on the work in [4] by replacing the far-field approximation with the more realistic near-field model, along with other subtle improvements. In order to use the proposed subsampling algorithm, it is necessary to linearize the model and solve for the antenna positions iteratively. Simulation results that do not yet consider various practical problems indicate that the algorithm works well. In future, practical effects such as mutual coupling between antenna elements in the array will be considered before moving on to applying the algorithm to practical data from the field.

8. Acknowledgments

This research received funding from the European Union's Horizon 2020 Research and Innovation Programme under the Marie Skłodowska-Curie grant agreement 101008231 (EXPOWER). It is also based on research supported in part by the National Research Foundation of South Africa (grant 75322), as well as the Netherlands Organisation for Scientific Research.

9. References

1. M. P. van Haarlem, M. W. Wise, A. W. Gunst, G. Heald, J. P. McKean, et al., "LOFAR: The Low-Frequency Array,"

Astronomy & Astrophysics, **556**, August 2013, p. A2, doi: 10.1051/0004-6361/201220873.
2. P. E. Dewdney, P. J. Hall, R. T. Schilizzi, and T. J. L. W. Lazio, "The Square Kilometre Array," *Proceedings of the IEEE*, **97**, 8, August 2009, pp. 1482-1496, doi: 10.1109/JPROC.2009.2021005.
3. S. J. Wijnholds, G. Pupillo, P. Bolli, and G. Virone, "UAV-Aided Calibration for Commissioning of Phased Array Radio Telescopes," 2016 URSI Asia-Pacific Radio Science Conference (URSI AP-RASC), Seoul, South Korea, August 21–25, 2016, pp. 228-231, doi: 10.1109/URSIAP-RASC.2016.7601375.
4. R. Louw, F. Knaepkens, A. Cuyt, W.-s. Lee, S. J. Wijnholds, et al., "Antenna Position Estimation Through Sub-Sampled Exponential Analysis of Harmonically Related Input Signals," 2021 XXXIVth General Assembly and Scientific Symposium of the International Union of Radio Science (URSI GASS), Rome, Italy, August 28–September 4, 2021, pp. 1-4, doi: 10.23919/URSIGASS51995.2021.9560519.
5. A. Cuyt, Y. Hou, F. Knaepkens, and W-s. Lee, "Sparse Multidimensional Exponential Analysis With an Application to Radar Imaging," *SIAM Journal on Scientific Computing*, **42**, 3, 2020, pp. B675-B695, doi: 10.1137/19M1278004.
6. M. Briani, A. Cuyt, F. Knaepkens, and W-s. Lee, "VEXPA: Validated EXPonential Analysis Through Regular Sub-Sampling," *Signal Processing*, **177**, December 2020, p. 107722, doi: 10.1016/j.sigpro.2020.107722.
7. A. Cuyt and W-s. Lee, "How to Get High Resolution Results From Sparse and Coarsely Sampled Data," *Applied and Computational Harmonic Analysis*, **48**, 3, May 2020, pp. 1066-1087, doi: 10.1016/j.acha.2018.10.001.
8. A. Barabell, "Improving the Resolution Performance of Eigenstructure-Based Direction-Finding Algorithms," ICASSP '83: IEEE International Conference on Acoustics, Speech, and Signal Processing, Boston, MA, USA, April 14–16, 1983, pp. 336-339, doi: 10.1109/ICASSP.1983.1172124.
9. G. Virone, P. Bolli, F. Paonessa, G. Pupillo, S. J. Wijnholds, et al., "Strong Mutual Coupling Effects on LOFAR: Modeling and In Situ Validation," *IEEE Transactions on Antennas and Propagation*, **66**, 5, May 2018, pp. 2581-2588, doi: 10.1109/TAP.2018.2816651.